FAILURE MECHANICS OF AN ENDODONTICALLY TREATED MAXILLARY FIRST PREMOLAR: A NUMERICAL ANALYSIS

Veronika Fedotova
Estevam Barbosa de las Casas
veronika.fedotova.a@gmail.com
estevam@dees.ufmg.br
Department of Structural Engineering, Universidade Federal de Minas Gerais
Av. Pres. Antônio Carlos, 6627, Pampulha, Belo Horizonte, 31270-901, Minas Gerais, Brazil
Osvaldo L. Manzoli
omanzoli@feb.unesp.br
Department of Civil Engineering, Universidade Estadual Paulista
Av. Eng. Luiz Edmundo C. Coube 14-01, Vargem Limpa, Bauru, 17033-360, São Paulo, Brazil
Claudia M.A. Mattos
cmamattos@gmail.com
Department of Dental Prosthodontics, Universidade Federal do Espirito Santo
Av. Marechal Campos, 1468, Maruípe, Vitória, 29040-090, Espirito Santo, Brazil
Eduardo A. Rodriguez
eduardoalex@feb.unesp.br
Department of Civil Engineering, Universidade Estadual Paulista
Av. Eng. Luiz Edmundo C. Coube 14-01, Vargem Limpa, Bauru, 17033-360, São Paulo, Brazil

Abstract. *The restoration of endodontically treated teeth is a widely studied, yet controversial topic in dentistry. Irreparable fracture is one of the most common causes of tooth loss after endodontic treatment. The present study aims to investigate the mechanics of failure of endodontically treated maxillary first premolar tooth restored by post-and-core and complete crown system, and explore the effect of adhesive bond failure on different material interfaces. The study is done using the finite element method employing the strategy named mesh fragmentation technique. The analysis revealed that, depending on the adhesive failure interface, cracks in dentin start to form with loads above 110 N. With pre-existing flaws in dentin, a load of 300 N was sufficient to provoke a catastrophic failure in all tested models.*

Keywords: *Endodontic treatment, Post-and-core, Root fracture, Damage model, Interface finite elements*

1. INTRODUCTION

Restoration of endodontically treated teeth is a widely studied, yet controversial topic in dentistry. Questions remain about the materials and clinical procedures to be applied, as irreparable fracture is one of the most common causes of tooth loss after endodontic treatment (Faria et al., 2011). Both sound and restored teeth may fracture, but endodontically treated teeth are more susceptible to fracture than vital teeth (Perez-Gonzalez et al., 2011), with weakness being attributed to altered or decreased tooth structure caused by caries, previous restorations, trauma, endodontic access and instrumentation, etc. (Schwartz&Robbins, 2004). The prognosis for weakened teeth strongly depends on the remaining tooth structure. When a coronal structure of a tooth is missing, a post-and-core restoration system is often necessary to retain the prosthetic crown (Robbins, 1990). Although some researchers believed in the past that posts could improve the fracture resistance in endodontically treated tooth, there are reports arguing that preparation of a post space may significantly weaken the root, thus increasing the chances of root fracture, as the occlusal stresses are transmitted directly through the core and post to the dentine; therefore the use of posts is currently undergoing serious debates (Milewsky&Chojnacka-Brozek, 2016; McComb, 2008). However, the posts are indicated for premolars to provide retention and resistance for the core material, and corono-radicular stabilization. An artificial post is adhesively cemented to the root walls and connects to the core, which retains the artificial crown, thereby transmitting the masticatory loads from the coronal structure to the root.

Fibre posts are bonded to dentine and core material, and their elastic modulus is similar to that of dentine (Newman et al., 2003). This can decrease stress concentration at the post apex (Aksornmuang et al., 2011). As fibre posts distribute stresses uniformly, they are less likely to cause root fractures (Perez-Gonzalez et al., 2011). Well dimensioned posts correctly positioned inside the root have good prognosis and are capable of withstanding expected masticatory loads. However, there are some factors that can lead to failure of this complex restoration, usually resulting in root fracture.

1.1. Possible failure modes of fibre post-and-core restorations

Dentine flaws or cracks leading to root fracture: Functional and parafunctional activity may lead to root fracture when there is a pre-existing flaw. Dentin has a fatigue limit (because of an inherent population of pre-existing flaws in normal dentin). For stresses smaller or equal to the normal stresses generated by mastication, flaw-free dentin apparently will not fail. However, if there is a pre-existing flaw of sufficient size (around 0.3 – 1.0 mm), it can grow to catastrophic proportion with cyclic loading even at stresses below 30 MPa (Kinney et al., 2003).

Failure of adhesive bonds leading to root fracture:

Polymerization shrinkage and contraction stress: Bonding to coronal dentin seems to be more predictable than to root canal dentin (Lopes et al., 2004). Besides, adhesive failures are not uncommon, because of the high sensibility of the adhesive technique and also as a result of the polymerization shrinkage of the composite luting cement and subsequent interface gap formation. Polymerization shrinkage and contraction stress of the resin were found to be a major cause of failure of composite restorations (Aksornmuang et al., 2011) and debonding of the core is the main failure mode of endodontic restorations (McLaren et al., 2009; Schmitter et al., 2010; Papadopoulos et al., 2010). Shrinkage stress is considered a multi-factorial phenomenon that can be affected by resin volume, cavity configuration, elastic modulus, and flow of resin composites. In the post space, the amount of resin composite is reduced when a fibre post is inserted into the cavity, resulting in lower contraction stress. On the other hand, the cavity configuration factor (C-factor), which represents the confinement area of the cavity, increases enormously after a fibre post is inserted. The restriction of free surfaces in such a deep and narrow canal would have a detrimental effect on the adhesion of the fibre post to root canal dentine, because of residual tensile shrinkage stresses (Aksornmuang et al., 2011). Hence, the cementation technique has shown to have a significant effect on the fracture strength (Schmitter, Rammelsberg et al., 2010), since the post dislodgement inside the root may cause a wedge effects that lead to root fracture. Failures of fibre posts were found to occur mainly due to loss of post retention (Marchionatti et al., 2017).

Insufficient resin cement polymerization: Dual-cured resin cements (simultaneous light and chemical polymerization curing modes) have been widely used in cementation of aesthetic posts. It was developed to overcome unfavourable characteristics of self-cured and light-cured resin cements. Nevertheless, when dual-cured resin is not exposed to light or light is attenuated, it has shown to decrease the degree of conversion (DC) (Braga et al., 2002). An insufficient DC of the resin may lead to unfavourable mechanical properties. Consequently, the solubility and permeability of resin cement layer to water can be challenged and its strength (Ho et al., 2011). During post cementation, light curing is impaired by the distance between the root walls and the light source. A decreased DC can lead to (a) low bond strength, and the subsequent microleakage could affect the adhesive properties of the post to root canal walls; and (b) poor mechanical properties and cohesive failure of the cement resulting in collapse of the cement layer.

Root fracture leading to failure of adhesive bonds: Although adhesive failure of the cement layer with subsequent loss of post retention and root fracture may be the most common failure mode, the opposite situation can also occur. In anatomically and histologically healthy teeth, the load applied to the crown is distributed within root dentin, transmitted to the surrounding ligament and then dissipated throughout the bone. The natural root is not structurally prepared to withstand loads directly applied to it. Inserting the post inside the root canal, which is normally filled by the soft pulp tissue, moves the load application site directly into the root internal walls, and this could cause root failures, particularly in structurally compromised roots with flared canals, or in the presence of a previous clinically non-detectable crack. Overloading from parafunctional activity can also contribute to root fracture in post-restored teeth. After root fracture, micromovements of the post associated with the leaking of soft tissue fluids will act in the dissolution of the cement layer and disintegration of adhesive bonds, resulting in post dislodgment.

Better understanding of crack formation mechanics in endodontically restored teeth may provide a valuable insight on the failure behaviour of post-and-core restoration systems. The aim of the present study is to investigate possible modes of crack formation and propagation in endodontically treated maxillary first premolar tooth restored by post-and-core and complete crown system. The study is done using finite element method (FEM) employing the strategy named mesh fragmentation technique, as proposed by Sánchez et al., 2014; Manzoli et al. (2012, 2013, 2016); and Rodrigues et al., 2016. This technique is described in detail below.

1.2. Mesh fragmentation technique using solid elements with high aspect ratio

Mesh fragmentation procedure: The strategy based on insertion of special finite elements between the regular elements of an original mesh is called "mesh fragmentation" by its authors (Sánchez et al., 2014; Manzoli et al., 2016; Rodrigues et al., 2016). In this technique, the original mesh is reassembled in such a manner that the regular elements are first transformed into independent elements by duplicating the shared nodes, and then a very small reduction is imposed on each element, creating narrow spaces between the elements. After that, the gap between the two neighbouring modified elements is filled by a pair of three-node triangular finite elements with high aspect ratio. Manzoli et al. (2012) refers to these degenerated elements as "interface solid elements" (ISE) or, for the sake of simplicity, simply as "interface elements" (IE).

Figure 1 illustrates the procedure adopted for mesh fragmentation; this procedure can be divided into three main steps:

1. Identification of a mesh to fragment and definition of new nodes in order to leave the original elements completely independent;
2. Reduction of each independent element imposing a very small displacement on its nodes in the direction of the center of gravity of the element;
3. Insertion of pairs of three-node finite elements with a high aspect ratio into the thin gaps created in steps 1 and 2.

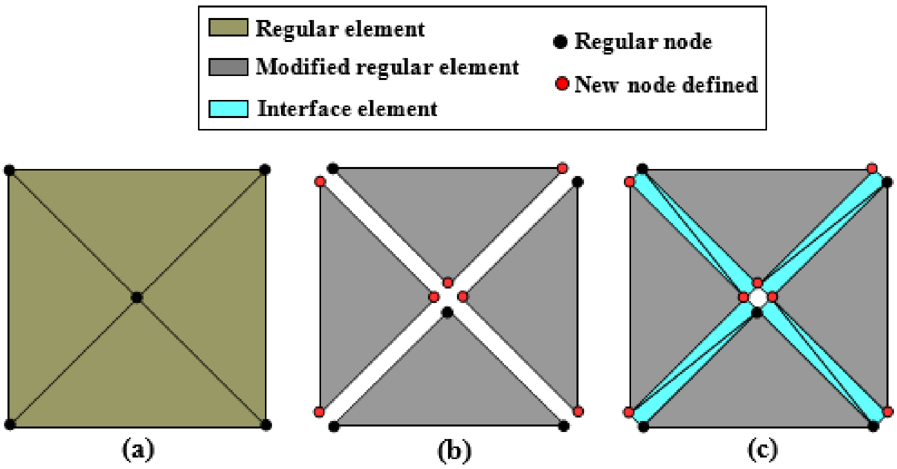

Figure 1. Mesh fragmentation technique: (a) original mesh, (b) duplication and reduction scheme (steps 1 and 2), and (c) introduction of IE (step 3)

Note that these IEs are defined from the modified regular elements' nodes. For the sake of comprehensiveness of the figure, the thickness of the gap between the elements shown in Fig. 1 is much greater than the one normally adopted (approximately 0.01 mm).

Brief formulation of the interface solid element: In recent work Manzoli and collaborators (2012) have shown that the strain tensor for any point of the interface element can be written in two parts: one bounded, ε, and another unbounded, $\hat{\varepsilon}$.

Proceedings of the XXXVIII Iberian Latin-American Congress on Computational Methods in Engineering
P.O. Faria, R.H. Lopez, L.F.F. Miguel, W.J.S. Gomes, M. Noronha (Editores), ABMEC, Florianópolis, SC, Brazil, November 5-8, 2017.

$$\boldsymbol{\varepsilon} = \tilde{\boldsymbol{\varepsilon}} + \hat{\boldsymbol{\varepsilon}} = \underbrace{\tilde{\boldsymbol{\varepsilon}}}_{\textbf{Bounded}} + \underbrace{\frac{1}{h}(\mathbf{n} \otimes \mathbf{u})^{s}}_{\textbf{Unbounded}} \tag{1}$$

The notation $(\boldsymbol{n} \otimes \boldsymbol{u})^s$ refers to the symmetric part of $(\boldsymbol{n} \otimes \boldsymbol{u})$; $\boldsymbol{n}$ is the unit vector normal to the element base; $\otimes$ denotes a dyadic product; and $\boldsymbol{u}$ is a vector of the components of the relative displacement, which according to the coordinate system adopted and showed in Fig. 2 are: $\boldsymbol{u_n}$ and $\boldsymbol{u_s}$.

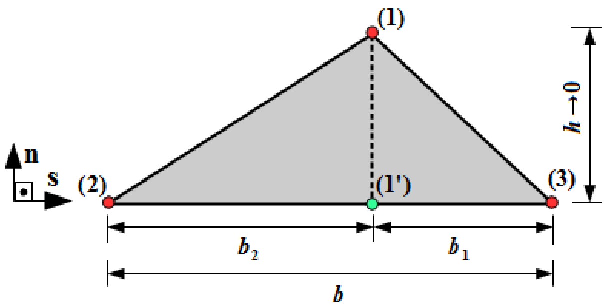

Figure 2. Triangular finite element with high aspect ratio

According to Eq. 1 and Fig. 2, when the height h tends to zero, the strain component ε remains bounded, while the component $\hat{\varepsilon}$ is no longer bounded. Therefore, in the limit situation of h tending to zero, the element strains are related almost exclusively to the relative displacement between node *(1)* and its projection on the element base, *(1')*. Thereby, in the limit situation, node *(1)* and its projection tend to the same material point. Consequently, the relative displacement $\boldsymbol{u}$ becomes the measure of a displacement discontinuity (strong discontinuity). The structure of the strain field in this equation corresponds to the typical kinematics of the Continuum Strong Discontinuity Approach (CSDA) (Oliver et al., 1999; Oliver and Huespe, 2004). Therefore, the same applications of the CSDA can be treated with triangular finite elements with high aspect ratio. Manzoli et al. (2012) demonstrate details about the equivalence between the strain field of the interface elements and kinematics of strong discontinuities.

1.3. Constitutive damage model

In this section, the constitutive models adopted to represent the behavior of the materials involved in the proposed approach are described. For the conventional IE of the fragmented mesh, a tension damage model is used. For the IE used between two different materials (IE used as a contact element), two combined damage models are applied: J2 and a tension damage model.

Tension damage model: To describe the nonlinear behaviour of the IE in tension, a constitutive damage model is used. The damage criterion is based on the component of tension stress, $\bar{\sigma}_{nn}$, normal to the base of the finite element with high aspect ratio. The model is formulated on the effective stress field associated with a scalar damage variable, $d \in [0.1]$, which is used to degrade all the components of effective stress tensor, $\bar{\boldsymbol{\sigma}}$, to calculate the nominal stress tensor, σ. Therefore, the proposed tension damage model can describe the crack initiation and propagation in mode I.

Table 1 shows general expressions of the tension damage model. More details about the formulation can also be found in Manzoli et al. (2016).

Table 1. Continuum constitutive equations for the tension damage model

	Constitutive tension damage model	
Effective stresses	$\bar{\boldsymbol{\sigma}} = \mathbf{C} : \boldsymbol{\varepsilon}$	(1)
Equivalent stress	$\bar{\tau} = \bar{\sigma}_{nn}$	(2)
Damage criterion	$\bar{\phi} = \bar{\tau} - r \leq 0$	(3)
Evolution law for the strain-type variable	$r(t) = r = \max\left[\bar{\tau}(s), f_t\right]$	(4)
Damage evolution	$d(r) = 1 - \frac{r}{f_t} e^{Ah\left(1-\frac{r}{f_t}\right)}$	(5)
Constitutive relation	$\boldsymbol{\sigma} = (1-d)\bar{\boldsymbol{\sigma}}$	(6)

In Eq. 2, ***C*** is the fourth order elastic tensor; ***ε*** is the second order strain tensor; and (*:*) is the tensorial product contracted in two indices.

According to Eq. 5, *r* assumes the maximum value that the effective stress $\bar{\sigma}_{nn}$ reaches during the loading process, starting from the initial tensile strength, f_t , of the material. The parameter *A* of Eq. 6 is related to the fracture energy, G_f , $A = (f_t^2)/(G_f E)$, and h is the thickness of the IE.

Combined damage model (J2 and Tension damage model): To represent the tangential (bond-slip) and normal nonlinear behavior of the IE between the different materials, a J2 damage model where the degradation criterion is based on the second invariant of the deviatoric part of the stress tensor (von Mises criterion), and the previously described tension damage model are used (combined) at the same time.

The J2 model is formulated on the effective stress field associated with a scalar damage variable, d^J *ϵ [0.1]*, which degrades only the deviatoric part of the effective stress. Thus, the constitutive relation of the J2 damage model can be written as:

$$\boldsymbol{\sigma}^J = \ 1 - d^J \ \ \bar{\boldsymbol{S}} + \bar{\boldsymbol{\sigma}}_V, \tag{8}$$

where $\bar{\boldsymbol{S}}$ and $\bar{\boldsymbol{\sigma}}_V$ are the deviatoric and the volumetric components of the effective stress tensor, such that:

Proceedings of the XXXVIII Iberian Latin-American Congress on Computational Methods in Engineering
P.O. Faria, R.H. Lopez, L.F.F. Miguel, W.J.S. Gomes, M. Noronha (Editores), ABMEC, Florianópolis, SC, Brazil, November 5-8, 2017.

$$\begin{cases} \bar{\boldsymbol{\sigma}} = \mathbf{C} : \boldsymbol{\varepsilon} \\ \bar{\boldsymbol{\sigma}} = \bar{\boldsymbol{S}} + \bar{\boldsymbol{\sigma}}_V \end{cases}, \tag{9}$$

where $\boldsymbol{C}$ is the fourth order linear-elastic constitutive tensor; $\boldsymbol{\varepsilon}$ is the second order strain tensor; and (:) is the tensorial product contracted in two indices.

The damage criterion can be expressed in terms of the effective stress as:

$$\bar{\phi}^J\left(\bar{\tau}^J, r^J\right) = \bar{\tau}^J - r^J \leq 0, \tag{10}$$

where r^J is the current damage threshold, and τ^J is the equivalent stress, given by:

$$\bar{\tau}^J = \frac{1}{\sqrt{2}}\left\| \bar{S} \right\| \tag{11}$$

The evolution of the damage threshold can be expressed in a closed form, always using the highest value reached by $\bar{\tau}^J$ during the loading process, i.e., $r^J = max(r_0^J, \bar{\tau}^J)$.

In this paper, the evolution of the damage variable assumes the following form:

$$d^J = 1 - \frac{q\left(r^J\right)}{r^J}, \tag{12}$$

where $q(r^J)$ is a function of the hardening/softening that can be calibrated from experimental tests or analytical expressions.

More details about this constitutive model can be found in Manzoli et al. (2012).

The composition of the models is done by first applying the J2 damage model, using as effective stress tensor the purely elastic stress tensor, calculated with the current strain tensor ($\bar{\boldsymbol{\sigma}} = \mathbf{C} : \boldsymbol{\varepsilon}$). Then the previously described tension damage model is used, assuming as effective stress for this model the stress tensor degraded by the J2 damage model ($\boldsymbol{\sigma}^J$), as follows:

$$\boldsymbol{\sigma} = (1-d)\boldsymbol{\sigma}^J = (1-d)\left[\left(1-d^J\right)\bar{\boldsymbol{S}} + \bar{\boldsymbol{\sigma}}_V\right] \tag{13}$$

Note that damage variable (d) derived from the tension damage model is applied to degrade all the components of the already degraded J2 current stress tensor. In this way, the IE used between the different materials can represent the material separation and a possible material slip, being suitable to simulate the contact effects between the materials.

To understand possible failure mechanics of a complex system, a two-dimensional (2D) simplification of the restored tooth model was employed in the study. It is believed that the 2D model can provide guidelines for further testing of a complete three-dimensional model, reducing the computational costs at the initial stages of tests, when multiple adjustments to the model are expected.

2. MATERIALS AND METHODS

A geometrical model of a maxillary first premolar used in the present work was adapted from a previously constructed model (Munari et al., 2015), which is based on computed tomography images. The geometry of a healthy first premolar and a part of the supporting maxillary bone were then modified in CAD software *Rhinoceros 5* (Robert McNeel & Associates, Seattle, USA) to include a one-post-and-core restoration system. A 15 mm long tapered glass fibre post with the coronal diameter of 1.25 mm, and the apical diameter of 0.92 mm was placed into the palatal root of the tooth so that the post would descend 2/3 of the root canal. A thin layer of cement was modelled around the post. The enamel from the original model was substituted by a complete ceramic crown, and a composite resin core restoration was added to partially replace the dentin in the model. To spare computational resources, no differentiation was done between the cortical and trabecular part of the supporting bone. The periodontal ligament (PDL) was preserved, and the vestibular canal entrance was filled with gutta-percha. A vertical cross-section of the created model was then used for a 2D representation of the problem, as shown in Fig. 3(a).

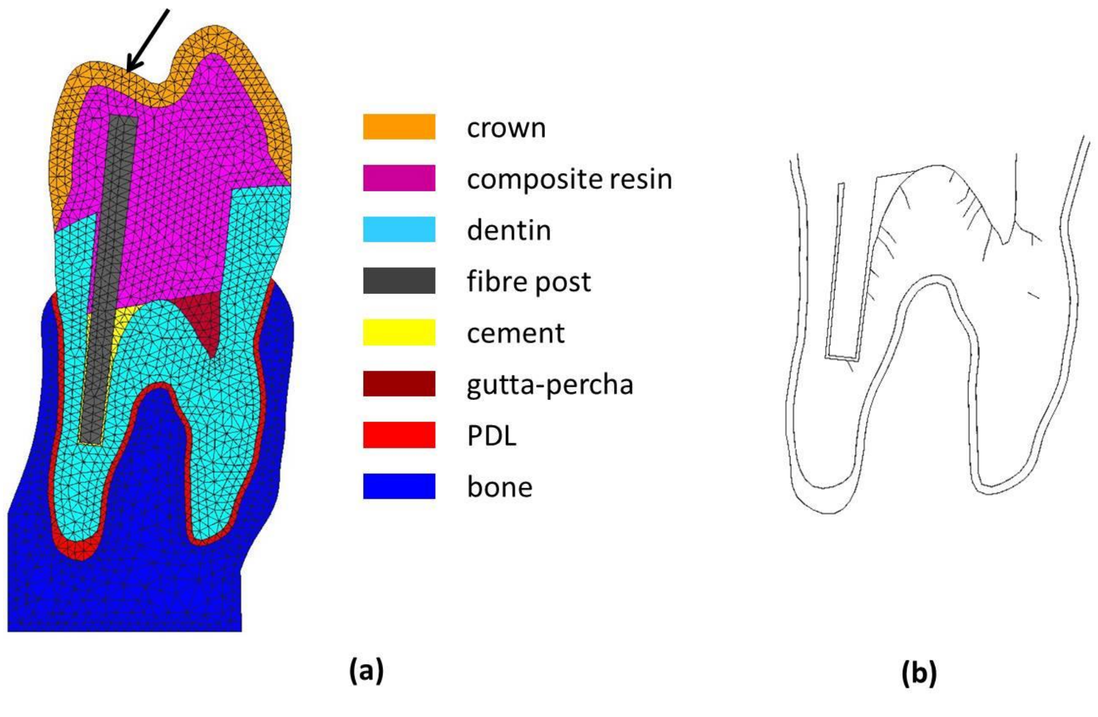

Figure 3. (a) 2D model of a maxillary premolar with post-and-core restoration with the applied load indicated by an arrow; (b) location of induced flaws in dentin (short lines around root canals)

Table 2 summarizes material properties used for the components of the model in accordance with Mattos et al. (2012), Chung et al. (2004), Lanza et al. (2005), Saskalauskaite et al. (2008), de Jager et al. (2004), Friedman et al. (1977), Kinney et al. (1999), Pietrzak et al. (2002), Baker et al. (2010), Reilly et al. (1974), Misch et al. (1999), van Staden et al. (2006), and Ferrari et al. (2010).

Table 2. Material properties of the components of the model

Material	Elastic modulus (GPa)	Poisson's ratio
Composite resin core	10.49	0.30
Glass fibre post	40	0.34
Resin cement	5.5	0.24
Gutta-percha	0.14	0.40
Dentin	18.45	0.29
Ceramic crown	82.3	0.22
Periodontal ligament (PDL)	0.31 e-04	0.45
Cortical bone	11.17	0.45

Pre- and post-processing of the model were done in GID (CIMNE, Barcelona, Spain) software. Interface elements were introduced into the mesh through the mesh fragmentation technique described above. To simulate pre-existing flaws in dentin, small cracks were introduced into the model; Fig. 3(b) shows localization of these cracks. A custom-made script was used to adopt various scenarios of possible adhesive bond failure between the materials and run the finite element analysis in Matlab (The MathWorks, Natick, USA) environment. Table 3 summarizes tested adhesive bond failure scenarios.

An oblique load up to 300 N simulating the occlusal forces was applied on the palatal surface of the crown as shown on Fig. 3(a). The nodes of the maxillary bone were restricted in all directions. The analysis was performed for crack formation and propagation loads.

Table 3. Tested adhesive bond failure scenarios

Scenario	Interface with an adhesive bond failure
1.	No adhesive failure
2.	Cement/dentin
3.	Cement/dentin, cement/post, and post/core
4.	Cement/dentin, cement/post, post/core, and core/dentin

3. RESULTS

Figures 4 to 7 show the results of numerical testing for crack formation in various adhesive bond failure scenarios. The applied load is shown for each case. Very small initial cracks are highlighted on the figures. Localization of the initial flaw incorporated into dentin is visible in Fig. 5(a), Fig. 6(a), and 7(a) as a darker magenta-coloured line.

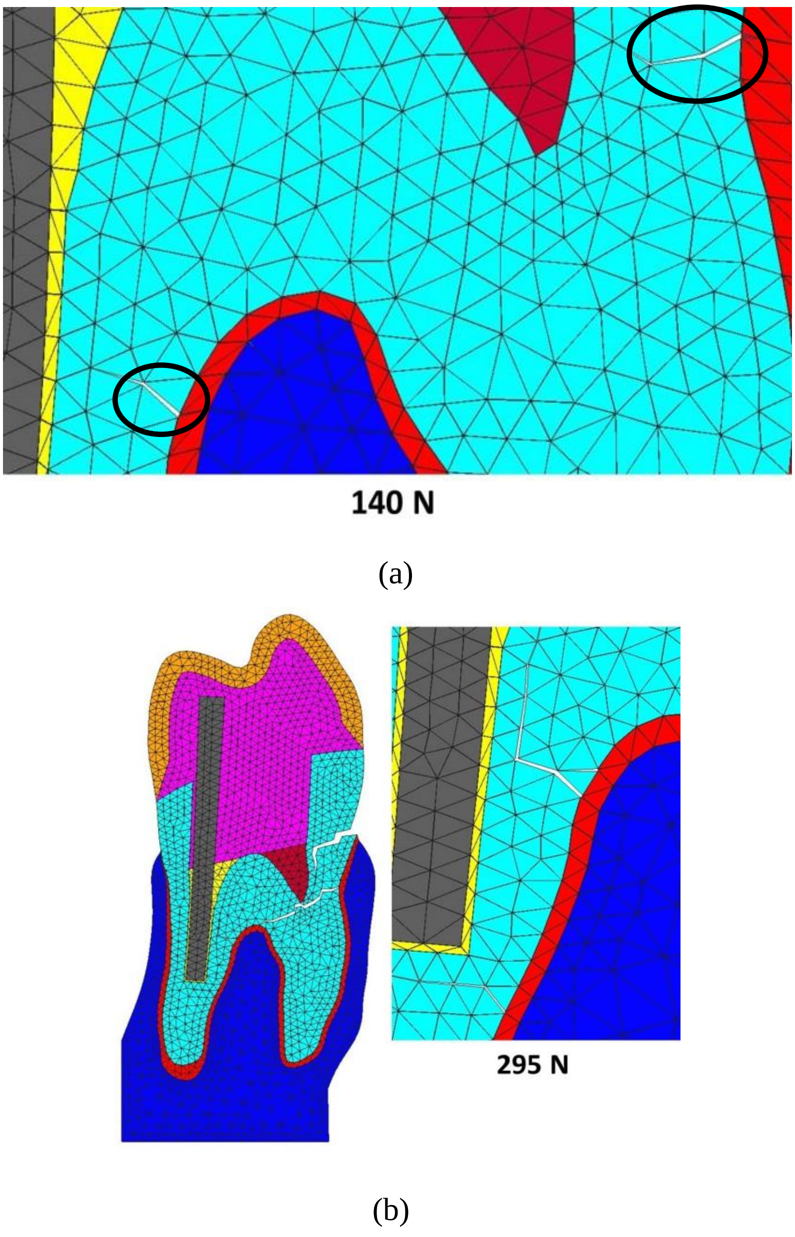

Figure 4. Crack formation in 1st scenario (no adhesive failure is permitted): (a) crack initiation; (b) crack propagation

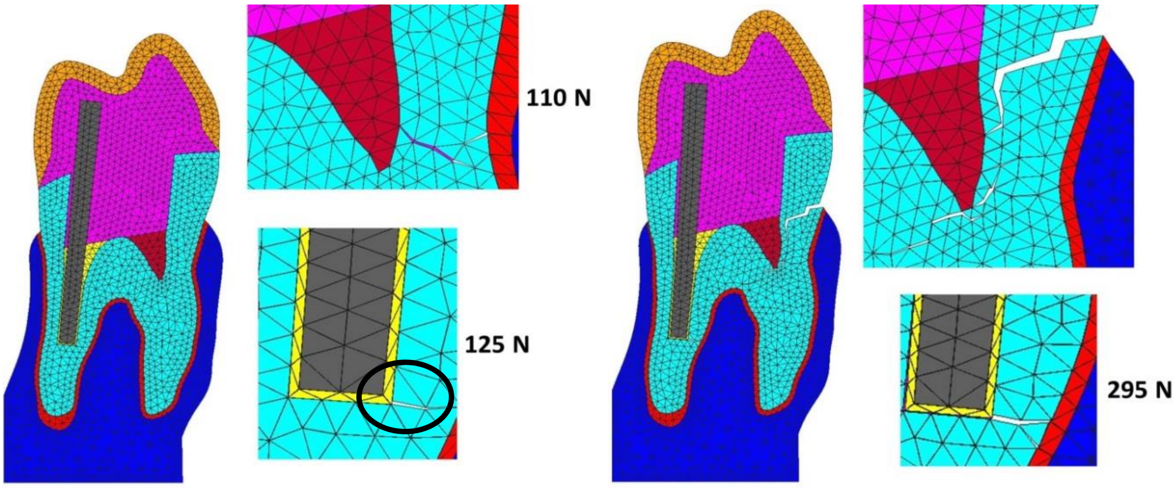

(a) (b)

Figure 5. Crack formation in 2nd scenario (adhesive bond failure on cement/dentin interface is possible): (a) crack initiation (initial flaw is highlighted); (b) crack propagation

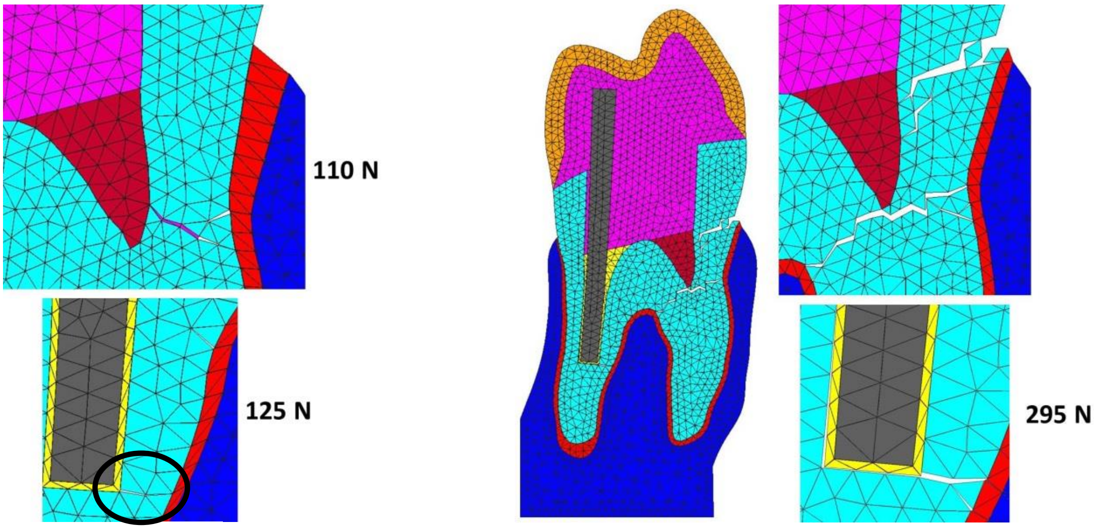

(a) (b)

Figure 6. Crack formation in 3rd scenario (adhesive bond failure is possible on cement/dentin, cement/post, and post/core interfaces): (a) crack initiation; (b) crack propagation

4. DISCUSSION

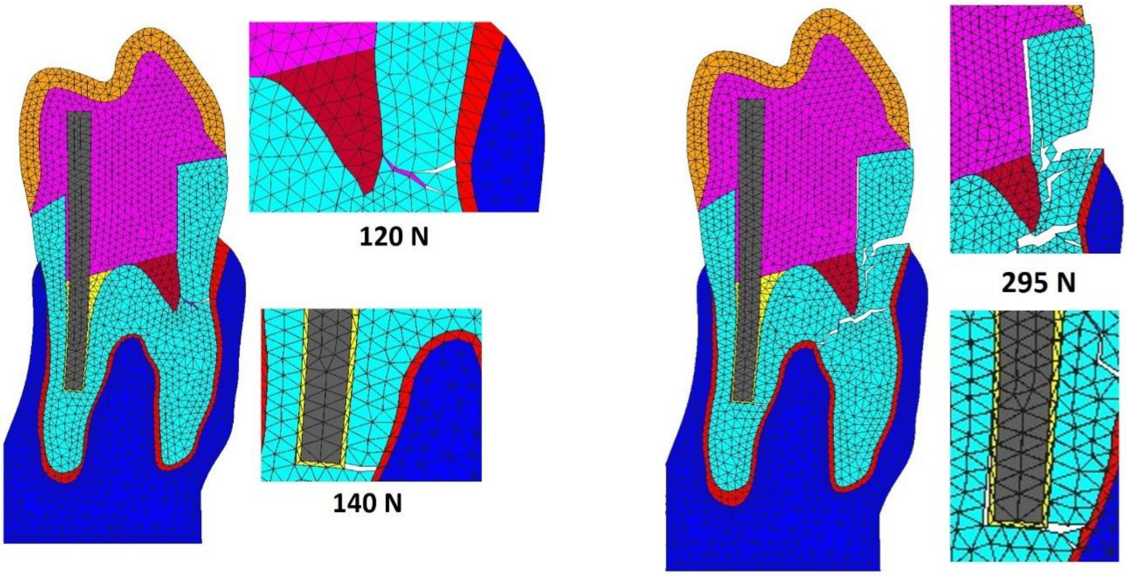

(a) (b)

Figure 7. Crack formation in 4th scenario (adhesive bond failure is possible on cement/dentin, cement/post, post/core, and core/dentin interfaces): (a) crack initiation; (b) crack propagation

Cracked teeth are a common and significant problem for patients and dentists (Lubisich et al., 2013), and are broadly classified as horizontal and vertical fractures (Malhotra et al., 2011).

In our study, a horizontal/oblique fracture of dentin was observed at loads around 300 N. It is interesting to note that the site of the main fracture is the same for all studied cases: dentin fractures at the cervical level on the vestibular side of the tooth, and the crack tends to propagate in a horizontal/oblique direction. This region of fracture agrees with the findings of Munari et al., 2015, which have shown that when oblique loads were applied on a numerical model of a healthy tooth, the higher stress concentration was observed at the cervical region and in the alveolar bone insertion.

For endodontically restored teeth, Hayashi et al., 2006, and Kumar & Rao, 2015 have demonstrated that under oblique loading such teeth are more likely to present a fracture at the cervical region if a fibre post is used, whilst vertical root fractures were associated with metal posts used in restoration. This behaviour was explained by the similarity of the elastic modulus of glass fibre post and that of dentin that would induce lower stress peaks inside the root. Metal post with high elastic modulus is more rigid and causes higher stress concentration at the apical third of the root.

Alsamadani et al., 2012, have also shown a horizontal cracking of dentin, however, in that study a vertical instead of oblique load was applied. Our study is limited to oblique loading and one type of material for post restoration, but the obtained cracking pattern is in agreement with previously published data for the chosen loading and restoration conditions.

Though the localization of main fracture is the same for all the analysed cases, each of the adhesive bond failure scenarios presents particularities regarding the development of other

Proceedings of the XXXVIII Iberian Latin-American Congress on Computational Methods in Engineering
P.O. Faria, R.H. Lopez, L.F.F. Miguel, W.J.S. Gomes, M. Noronha (Editores), ABMEC, Florianópolis, SC, Brazil, November 5-8, 2017.

fractures, which suggests an important role of adhesive bonding conditions between restoration materials. In the scenarios 2 to 4, the first crack in dentin started at the proximity of the pre-existing flaw next to vestibular canal entrance, which is most likely attributed to the weakened dentin; a slightly higher load was needed to induce the second crack, localized in the palatal root. In case of the system with no adhesive failure (1^{st} scenario), the cracks in the vestibular and palatal root started to form almost simultaneously, and, when compared to other cases, a higher load was necessary to initiate the formation of these cracks. When there are no defects in bonding between the elements of such a complex biomechanics system as a restored tooth, a higher fracture resistance would be expected, as the stresses are distributed more evenly between the materials.

In all cases the initial crack on the vestibular side propagated horizontally, at higher loads eventually leading to the separation of the vestibular root from the rest of the tooth. As the load reached 295 N, this separation occurred in cases 1, 3, and 4. In the 2^{nd} scenario, where only the cement/dentin bond failure was allowed, this secondary crack propagation was not high enough to cause a total disruption of the root at this load magnitude. However, to spare the computational resources and avoid a very fine meshing of a thin apical end of the root canals while modelling the tooth, the canals were shortened, so that in the vestibular root only the canal entrance is represented. Therefore, the observed separation of the whole vestibular root might be rather a result of this model limitation.

When the separation of the core from the dentin was permitted (4^{th} scenario) a more dramatic degradation of the tooth was observed: besides the fracture at the cervical region of the vestibular root, the disintegration of the tooth is apparent, with part of the dentin being separated from the rest of the tooth structure. Although it has been demonstrated that core debonding was the predominant failure mode for glass fibre post restorations (Papadopoulos et al., 2010), this failure mode can be considered a repairable fracture, different from root fracture, which inevitably condemns the tooth to extraction.

From Fig. 4 – 7, it can be observed that on the palatal root near the post, the cracks propagated at a slower rate than on the vestibular side, despite the presence of the pre-existing flaws in both roots. The cracks initiating from the apical end of the post only appeared when the adhesive bond failure on dentin/cement interface was possible (scenarios 2, 3, and 4). In the perfect bonding case the crack would appear around the induced flaws. The importance of good adhesion between the cement and the dentin has been previously demonstrated (Lin & Douglas, 1994; de Santis et al., 2000); the cement bulk is expected to preserve the dentin from dangerous stress accumulation.

The importance of ferrule effect on fracture resistance of endodontically restored teeth is widely accepted (McComb, 2008). In the present study, no ferrule was included into the restored geometry. The absence of ferrule together with the introduced flaws in dentin could explain the relatively low loads needed to induce fractures in the analysed models.

5. CONCLUSIONS

FEM studies simulate the behavior of a specific model and do not necessarily conform to the biologic structures; however, the results obtained from numerical simulations provide better understanding of the underlying mechanics in a more generalized way. The performed analysis has demonstrated the influence of adhesive bond failure modes on the crack propagation in endodontically treated teeth. Though restricted to 2D analysis, and presenting several geometric limitations, the analyzed situations provide an insight into the behavior of restored tooth under loading conditions.

Acknowledgements

The authors gratefully acknowledge the important support of the Brazilian research agency FAPEMIG (in Portuguese "Fundação de Amparo à Pesquisa do Estado de Minas Gerais"), CNPq and CAPES foundation.

REFERENCES

Aksornmuang, J., Nakajima, M., Senawongse, P., & Tagami, J., 2011. Effects of C-factor and resin volume on the bonding to root canal with and without fibre post insertion. *Journal of Dentistry*, vol. 39, iss. 6, pp. 422 – 429.

Baker, M. I., Eberhardt, A. W., Martin, D. M., McGwin, G., & Lemons, J. E., 2010. Bone properties surrounding hydroxyapatite-coated custom osseous integrated dental implants. *Journal of Biomedical Materials Research Part B: Applied Biomaterials*, vol. 95, n. 1, pp. 218 – 224.

Braga, R. R., Cesar, P. F., & Gonzaga, C. C., 2002. Mechanical properties of resin cements with different activation modes. *Journal of Oral Rehabilitation*, vol. 29, iss. 3, pp. 257 – 262.

Chung, S. M., Yap, A. U., Koh, W. K., Tsai, K. T., & Lim, C. T., 2004. Measurement of Poisson's ratio of dental composite restorative materials. *Biomaterials*, vol. 25, n. 13, pp. 2455 – 2460.

de Jager, N., Pallav, P., & Feilzer, A. J., 2004 The apparent increase of the Young's modulus in thin cement layers. *Dental Materials*, vol. 20, n. 5, pp. 457 – 462.

de Las Casas E. B., Manzoli O. L., & Mattos C. M. A., 2014. Crack propagation in post-core rehabilitation of a maxillary central incisor after root reconstruction. In Blucher Mechanical Engineering Proceedings, *10th World Congress on Computational Mechanics (10th WCCM)*, pp. 2919 – 2929.

de Santis, R., Prisco, D., Apicella, A., Ambrosio, L., Rengo, S., & Nicolais, L., 2000. Carbon fiber post adhesion to resin lutin cement in the restoration of endodontically treated teeth. *Journal of Materials Science: Materials in Medicine*, vol 11, iss. 4, pp. 201 – 2016.

Faria, A. C. L, Rodrigues, R. C. S., Antunes, R. P. de A, de Mattos, M. G. C., & Ribeiro, R. F., 2011. Endodontically treated teeth: Characteristics and considerations to restore them. *Journal of Prosthodontic Research*, vol. 55, pp. 69 – 74.

Ferrari, E. M. M., Hickel, R., & Ilie, N., 2010. Evaluation of the mechanical properties of dental adhesives and glass-ionomer cements. *Clinical Oral Investigations*, vol. 14, iss. 1, pp. 79 – 87.

Friedman, C. E., Sandrik, J. L., Heuer, M. A., & Rapp, G. W., 1977. Composition and physical properties of gutta-percha endodontic filling materials. Journal of Endodontics, vol. 3, n. 8, pp. 304 – 308.

Hayashi, M., Takahashi, Y., Imazato, S., & Ebisu, S., 2006. Fracture resistance of pulpless teeth restored with post-cores and crowns. *Dental Materials*, vol. 22, n. 5, pp. 477 – 485.

Ho, Y. C., Lai, Y. L., Chou, I. C., Yang, S. F., & Lee S. Y., 2011. Effects of light attenuation by fibre posts on polymerization of a dual-cured resin cement and microleakage of post-restored teeth. *Journal of Dentistry*, vol. 39, iss. 4, pp. 309 – 315.

Alsamadani, K. H., Abdaziz, el-S. M., & Gad, el-S., 2012. Influence of Different Restorative Techniques on the Strength of Endodontically Treated Weakened Roots. *International Journal of Dentistry*, v. 2012.

Kinney, J. H., Balooch, M., & Marshall, G. V., 1999. A micromechanics model of the elastic properties of human dentine. *Archives of Oral Biology*, vol. 44, n. 10, pp. 813 – 822.

Kinney, J. H., Marshall, S. J., & Marshall, G. W., 2003. The mechanical properties of human dentin: a critical review and re-evaluation of the dental literature. *Critical Reviews in Oral Biology & Medicine*, vol. 14, n. 1, pp. 13 – 29.

Kumar, P., & Rao, R. N., 2015. Three-dimensional finite element analysis of stress distribution in a tooth restored with metal and fiber posts of varying diameters: An in-vitro study. *Journal of Conservative Dentistry*, v. 18, iss. 2, pp. 100 – 104.

Lanza, A., Aversa, R., Rengo, S., Apicella, D., &Apicella, A., 2005. 3D FEA of cemented steel, glass and carbon posts in a maxillary incisor. *Dental Materials*, vol. 21, n. 8, pp. 709 – 715.

Lopes, G. C., Cardoso, P. de C, Vieira, L. C., & Baratieri, L. N., 2004. Microtensile bond strength to root canal vs pulp chamber dentin: effect of bonding strategies. *The Journal of Adhesive Dentistry*, vol. 6, iss. 2, pp. 129 – 133.

Lubisich, E. B., Hilton, T. J., & Ferracane, J., 2013. Cracked Teeth: A Review of the Literature. *Journal of Esthetic and Restorative Dentistry*, vol. 22, iss. 3, pp. 158 – 167.

Malhotra, N., Mala, K., & Acharaya, S. R., 2011. Resin-based composite as a.direct esthetic restorative material. *Compendium of Continuing Education in Dentistry*, vol. 32, iss. 5., pp. 14 – 23.

Manzoli, O. L., Claro-Bazucco, G. K. s., Rodrigues, E. A, & Lopes Jr, J. A., 2013. A local-global scheme for tracking crack path in three-dimensional solids. *Computers and Concrete*, vol. 12, n. 3, pp. 261 – 283.

Manzoli, O. L., Gamino, A. L., Rodrigues, E. A., & Claro-Bazucco, G. K. s., 2012. Modeling of interfaces in two-dimensional problems using solid finite elements with high aspect ratio. *Computers and Structures*, vols. 94-95, pp. 70 – 82.

Manzoli, O. L., Maedo, M. A., Bitencourt Jr, L. A. G., & Rodrigues, E. A., 2016. On the use of finite elements with high aspect ratio for modeling cracks in quasi-brittle materials. *Engineering Fracture Mechanics*, vol. 153, pp. 151 – 170.

Marchionatti, A. M. E., Wandscher, V. F., Rippe, M. P., Kaizer, O. B., & Valandro, L. F., 2017. Clinical performance and failure modes of pulpless teeth restored with posts: a systematic review. *Brazilian Oral Research*, vol. 31, e64.

Mattos, C. M., de Las Casas, E. B., Dutra, I. G., Sousa, H. A., & Guerra, S. M., 2012. Numerical analysis of the biomechanical behaviour of a weakened root after adhesive reconstruction and post-core rehabilitation. *Journal of Dentistry*, vol. 40, pp. 423 – 432.

McComb, D., 2008. Restoration of the endodontically treated tooth. In *PEAK Supplement to Dispatch February/March 2008*, pp. 1 – 20. Royal College of Dental Surgeons of Ontario.

McLaren, J. D., McLaren, C. I., Yaman, P., Bin-Shuwaish, M. S., Dennison, J. D., & McDonald, N. J., 2009. The effect of post type and length on the fracture resistance of endodontically treated teeth. *Journal of Prosthetic Dentistry*, vol. 101, iss. 3, pp. 174 – 182.

Milewski, G., & Chojnacka-Brozek, A., 2016. Strength analysis of catastrophic root fractures for endodontically treated lateral teeth. In *24th International Congress on Theoretical and Applied Mechanics (XXIV ICTAM)*.

Misch, C. E., Qu, Z., & Bidez, M. W., 1999. Mechanical properties of trabecular bone in the human mandible: implications for dental implant treatment planning and surgical placement. *Journal of Oral and Maxillofacial Surgery*, vol. 57, n. 6, pp. 700 – 708.

Munari, L. S., Moreira, A., de las Casas, E. B. & Magalhaes, C. S., 2015. Stress distribution in a premolar 3D model with anisotropic and isotropic enamel. *Medical&Biological Engineering&Computing*, vol. 53, iss. 8, pp. 751 – 758.

Newman, M. P., Yaman, P., Dennison, J., Rafter, M., & Billy, E., 2003. Fracture resistance of endodontically treated teeth restored with composite posts. *Journal of Prosthetic Dentistry*, vol. 89, iss.4, pp. 360 – 367.

Oliver, J. & Huespe, A., 2004. Continuum approach to material failure in strong discontinuity settings. *Computer Methods in Applied Mechanics and Engineering*, vol. 193, pp. 3195–3220.

Oliver, J., Cervera, M., & Manzoli, O. L., 1999. Strong discontinuities and continuum plasticity model: the strong. discontinuity approach. *International Journal of Plasticity*, vol. 15, pp. 319 – 351.

Papadopoulos, T., Papadogiannis, D., Mouzakis, D. E., Giannadakis, K., & Papanicolaou, G, 2010. Experimental and numerical determination of the mechanical response of teeth with reinforced posts. *Biomedical Materials*, vol. 5, iss. 3, 35009.

Perez-Gonzalez, A., Gonzalez-Lluch, C., Sancho-Bru, J. L., Rodriguez-Cervantes, P. J., Barjau-Escribano, A., & Forner-Navarro, L., 2012 Experimental strength of restorations with fibre posts at different stages, with and without using a simulated ligament. *Journal of Oral Rehabilitation*, vol. 39, iss. 3, pp. 188 – 197.

Pietrzak, G., Curnier, A., Botsis, J., Scherrer, S., Wiskott, A., & Belser, U., 2002. A nonlinear elastic model of the periodontal ligament and its numerical calibration for the study of tooth mobility. *Computer Methods in Biomechanics and Biomedical Engineering*, vol. 5, n. 2, pp. 91 – 100.

Reilly, D. T., & Burstein, A. H., 1974. Review article. The mechanical properties of cortical bone. *The Journal of Bone and Joint Surgery – Americal Volume*, vol. 56, n. 5, pp. 1001 – 1022.

Robbins, J. W., 1990. Guidelines for the restoration of endodontically treated teeth. *Journal of the American Dental Association*, vol. 120, iss. 5, pp. 558, 60, 62, 64, 66.

Rodrigues, E. A., Manzoli, O. L., Bitencourt Jr., L. A. G., & Bittencourt, T. N., 2016. 2D mesoscale model for concrete based on the use of interface element with a high aspect ratio. *International Journal of Solids and Structures*, vol. 94, pp. 112 – 124.

Sánchez, M., Manzoli, O. L., & Guimarães, L. J. N., 2014. Modeling 3-D desiccation soil crack networks using a mesh fragmentation technique. *Computers and Geotechnics*, vol. 62, pp. 27 – 39.

Saskalauskaite, E., Tam, L. E., & McComb, D., 2008. Flexural strength, elastic modulus, and pH profile of self-etch resin luting cements. *Journal of Prosthodontics*, vol. 17, n. 4, pp. 262 – 268.

Schmitter, M., Lippenberger, S., Rues, S., Gilde, H., & Rammelsberg, P., 2010. Fracture resistance of incisor teeth restored using fibre-reinforced posts and threaded metal posts: effect of post length, location, pretreatment and cementation of the final restoration. *International Endodontic Journal*, vol. 43, iss. 5, pp. 436 – 442.

Schmitter, M., Rammelsberg, P., Lenz, J., Scheuber, S., Schweizerhof, K., & Rues, S., 2010. Teeth restored using fiber-reinforced posts: in vitro fracture tests and finite element analysis. *Acta Biomaterialia*, vol. 6 iss. 9, pp. 3747 – 3754.

Schwartz, R. S., & Robbins, J. W., 2004. Post placement and restoration of endodontically treated teeth: a literature review. *Journal of Endodontics*, vol. 30, iss. 5, pp. 289 – 301.

Van Staden, R. C., Guan, H., & Loo, Y. C., 2006. Application of the finite element method in dental implant research. *Computer Methods in Biomechanics and Biomedical Engineering*, vol. 9, n. 4, pp. 257 – 270.